Partial Wetting Phenomenon in Superhydrophobic Microchannels

Report Contributors: Karl Borg[1], Vincent Cregan[1,2], Andrew Fowler[1], Mark McGuinness[1,3], Stephen B.G. O'Brien[1], Leonard W. Schwartz[4] and Vladimir Zubkov[1]

Industry Representatives:
Niall O'Keefe[5], Ryan Enright[5] and Cormac Eason[5]

[1]MACSI, Department of Mathematics and Statistics, University of Limerick, Ireland
[2]Report coordinator, vincent.cregan@ul.ie
[3]School of Mathematics, Statistics and Operations Research, Victoria University of Wellington, New Zealand
[4]Department of Mechanical Engineering, University of Delaware, United States of America
[5]Stokes Institute, University of Limerick, Ireland

1 Introduction

Superhydrophobic surfaces are a class of materials that display extreme wetting behaviour that can result in almost spherical liquid droplets. For superhydrophobic surfaces the contact angle between the liquid and the surface may be much greater than 90°. This extreme wetting behaviour is a direct result of a favourable surface potential combined with surface micro/nano-structures. A high degree of surface roughness can lead to a significant increase in the contact angle compared to a smooth surface[1].

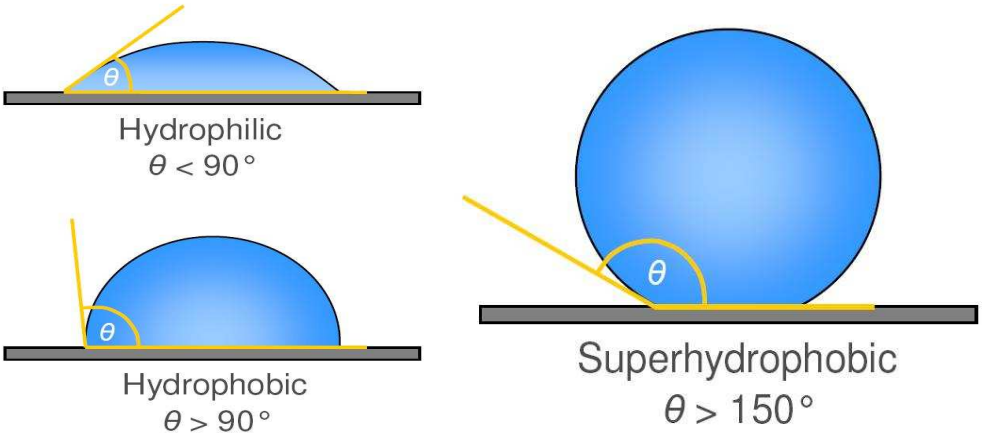

Figure 1: Overview of various liquid drop orientations on a surface.

(a) Lotus leaf (b) Water strider

Figure 2: Examples of superhydrophobic surfaces in nature.

The leaves of the lotus plant[2] and the lady's mantle[3] are well-known examples of superhydrophobic surfaces in nature. Microstructues on the surface of the lotus leaf allows the leaf

to be self-cleaning and strongly repellent to water droplets. Superhydrophobicity is not restricted just to the plant world. Water striders posses superhydrophobic legs which allow them to walk along the surface of water and the wings of many butterflies have superhydrophobic properties[3].
An understanding of superhydrophobic wetting behaviour is of huge importance in industry and the phenomenon has received much attention in the last decade due to the proliferation of microfabrication techniques allowing large areas of geometrically well defined surface structures to be produced. Superhydrophobic surfaces are used in the design of waterproof clothing raincoats, windscreens and satellite dishes. Superhydrophobic surfaces are currently playing a major role in the fabrication of silicon wafers[3] via fluidic self-assembly. Another application of these surfaces is as liquid flow boundaries in microfluidics. It has been shown analytically, numerically, and experimentally that superhydrophobic surfaces can produce an apparent slip effect due to reduced liquid/solid interaction and the presence of a trapped gas/vapour layer at the superhydrophobic surface.

The Stokes Institute are currently using superhydrophobic surfaces in a number of their experiments. In one particular experimental process, a syringe pump is used to force deionised water through a parallel plate microchannel. The microchannel inlet and outlet are connected to two large fluid reservoirs. The upper wall is a flat no-slip surface while the lower wall is a superhydrophobic surface made up of small cylindrical pillars.

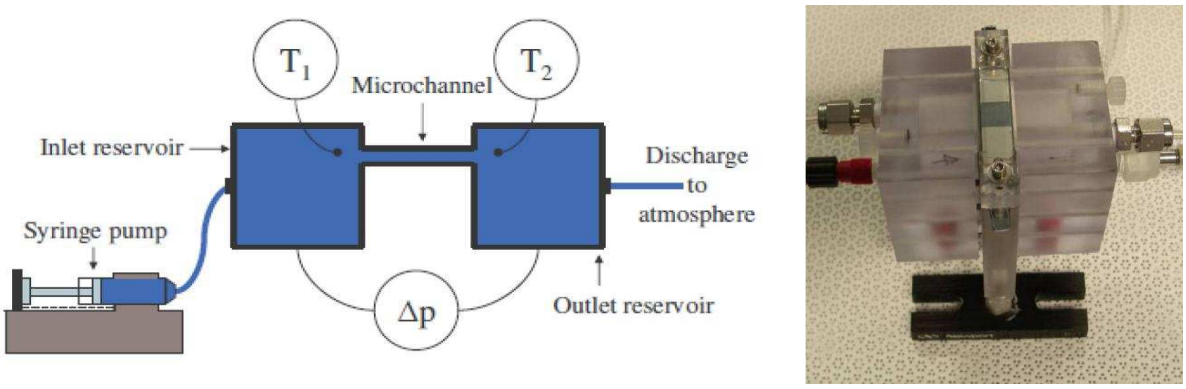

(a) Microchannel schematic (b) Experimental apparatus

Figure 3: Overview of experimental setup.

The breadth, length and height of the microchannel is 10mm, 10mm and $80\mu\text{m}$, respectively. Pillar dimensions vary depending on the type of experimental setup but for this report we will use $7.5\mu\text{m}$ and $25\mu\text{m}$ as values for the pillar radius and height, respectively. The distance between two pillars (centre to centre) is $20\mu\text{m}$. The velocity of the water as it passes through the microchannel is 0.012ms^{-1}. [4] contains a detailed description of the experimental apparatus.

As the water passes through the microchannel, air gets trapped between the pillars and the

water. This segregated two-phase flow exists due to surface tension. The stability of the flow structure is controlled primarily by the geometry of the superhydrophobic surface structures. Assuming equilibrium conditions, energy-based calculations performed provide criteria for the stability of the wetting regime and have been validated experimentally in droplet experiments. However, recent experimental investigation performed by Stokes have demonstrated the existence of a 'partial' wetting state on pillar-structured superhydrophobic surfaces that is not predicted by equilibrium analysis. The partial wetting state has been observed using direct imaging of the superhydrophobic surfaces located in a Hele-Shaw microchannel using laser-scanning confocal microscopy and shows that the gas/liquid/solid contact line forms some distance from the top of the pillar structures upon filling of the microchannel. Typically, the contact line has been found $10-15\mu$m below the pillar tops. In addition, the height of the contact line varies from pillar to pillar. Investigation of the pillar structures using SEM (Scanning electron microscope) has shown that the pillar sides are not smooth, but instead demonstrate scallop features, which are a result of the fabrication process. These scallop features represent contact-line pinning sites that are not captured in existing energy calculations, which can explain why the pillars remain partially wetted. However, it is unknown why this partial wetting phenomenon should occur in the first place and it does not appear to have been described in the literature prior to Stokes' experimental work.

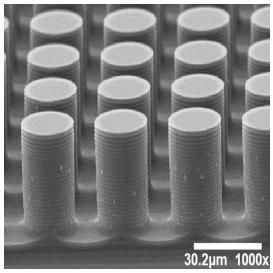

(a) Pillars on superhydrophobic surface

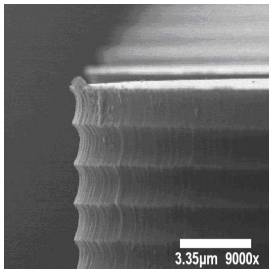

(b) Pillar scallops

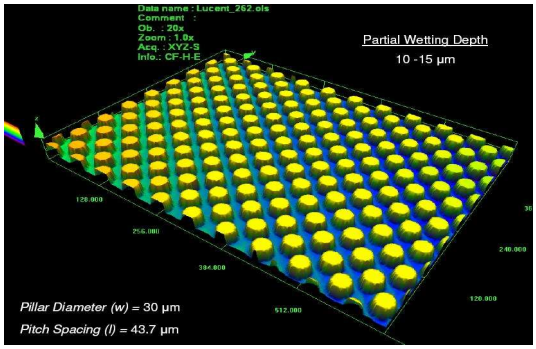

(c) Confocal image of liquid interface in contact with pillars.

Stokes are interested in mathematical modelling their experimental set-up and understanding

the physical mechanisms involved in their experiment. An understanding of these mechanisms, developed through modelling, is of particular interest for informing the design of future devices. The key problems to be studied may be summarised as follows:

- **Problem 1:** Describe the mechanism behind liquid penetration of the pillars. What is the cause of the liquid going $10-15\mu$m down along the pillars? Why does the liquid drop height vary from pillar to pillar?
- **Problem 2:** How do the scallops affect the contact line pinning of the liquid?

The modelling work performed during the study group is summarised in this report. The report is split into six main sections and suggestions for future work are found in the concluding section. The content of the sections may be summarised as follows:

- **Section 2:** Review of possible surface wetting surface states
- **Section 3:** Time scales involved in problem
- **Section 4:** Height of water-air interface drop in contact with single cylindrical pillar
- **Section 5:** Partial wetting phenomenon in superhydrophobic microchannels in two dimensions
- **Section 6:** Poiseuille flow across pillars

2 Surface wetting states

Young's equation relates the thermodynamic equilibrium contact angle, θ_c of a liquid drop to the specific energies of the surface-liquid, surface-air and liquid-air interfaces[5]

$$\gamma_{SG} = \gamma_{SL} + \gamma_{LG} \cos\theta_C$$

γ_{ij} denotes the specific energy between medium i and medium j. However, Young's equation is restricted to smooth, flat surfaces. It was recognised early that surface roughness may lead to deviations in the contact angle predicted by Young's equation. In the literature, Wenzel's seminal work was to first to describe the impact of surface roughness and superhydrophobic wetting behaviour in the context of waterproofing of knitted fabrics[7]. Wenzel illustrated how a rough surface can increase the apparent contact angle at the boundary between a liquid and a surface. Wenzel related the standard Young contact angle, θ_C to the contact angle on the rough surface, θ_W by the formula

$$\cos\theta_W = r \cos\theta_C$$

where r is a roughness factor. When a liquid drop occupies the spaces between the surface projections, the drop is said to be in the Wenzel state.

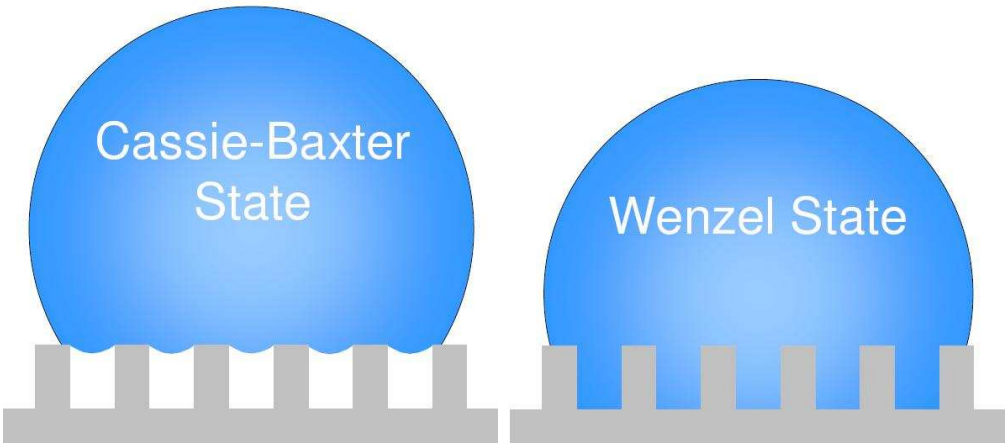

Figure 4: Overview of various liquid drop orientations on a superhydrophobic surface with topography.

Cassie and Baxter extended Wenzel's work by considering the wettability or water-repellency of porous surfaces such as natural and artificial clothing[8]. In the Cassie-Baxter (or Fakir) state, a liquid drop remains balanced on the surface projections with air trapped underneath.

The associated equilibrium condition is

$$\cos\theta_{CB} = \Phi\left(\cos\theta_C + 1\right) - 1$$

where Φ is the solid fraction of the surface. [6] contains a detailed description of the various wetting states associated with superhydrophobic surfaces.

3 Problem timescales

In this section we discuss some of the timescales relevant to the problem. The Stokes Institute advise that it takes about one second for the water to traverse the top of the pillars, with an associated velocity of 10mm s^{-1}. It is of interest to consider how quickly air that is caught between the water and the bottom of the pillar array can escape through the pillar array.

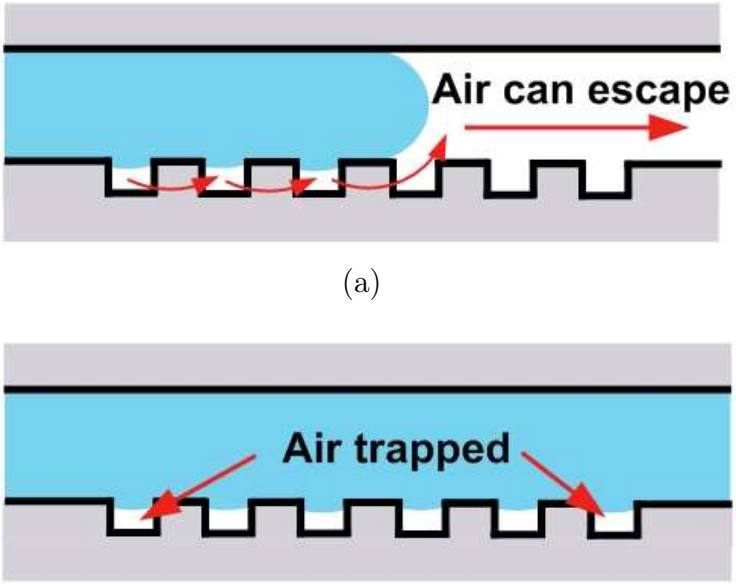

(a)

(b)

Figure 5: (a) As the water moves through the microchannel, air is free to move around the pillars and escape. (b) Air gets trapped between the water and the pillars once the water has passed completely through the microchannel.

Treating the array as a porous medium, with a porosity of 0.6 calculated from the geometry, Darcy's law gives the volume flux (ms^{-1})

$$q = \frac{k}{\mu_g}\nabla p$$

where the dynamic viscosity of air is $\mu_g = 1.8 \times 10^{-5}\text{kgm}^{-1}\text{s}^{-1}$ at $20°\text{C}$, and the pressure difference used in the experiments to drive the water, taken to be also driving air flow, is typically about 100Pa over 10mm, so that $\nabla p \approx 10^4\ \text{Pam}^{-1}$. The permeability is the most uncertain parameter. Here we will use two different ways to estimate k, permeability-porosity plots from hydrogeology and the more formal Carmen-Kozeny relationship.

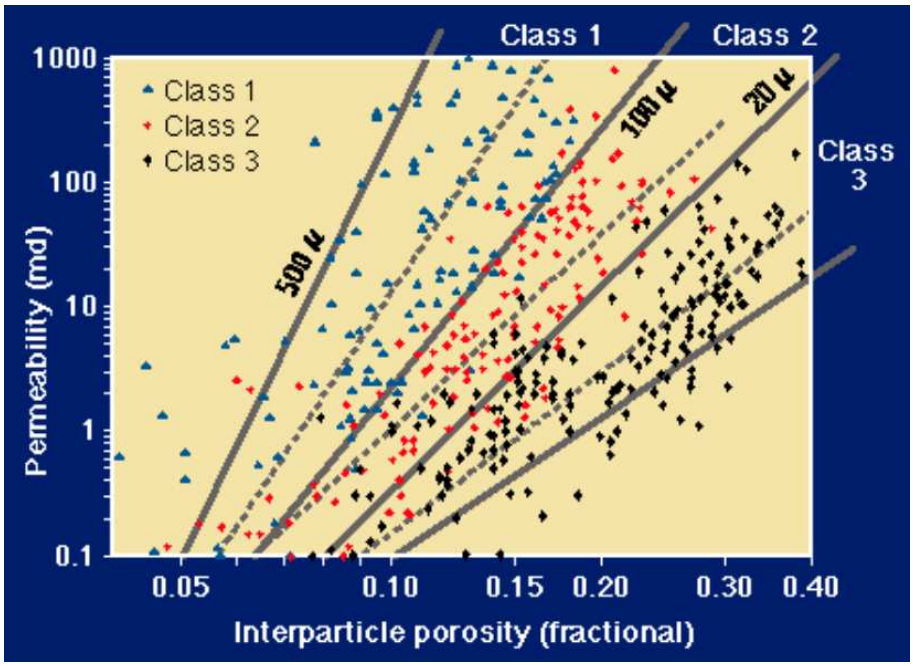

Figure 6: A porosity-permeability plot, from the Bureau of Economic Geology, University of Texas at Austin. The lines indicate pore sizes.

Using the permeability-porosity cross plot illustrated in figure (6), the relationship between porosity and permeability for rocks depends on the average pore dimension also. Using the line corresponding to a $20\,\mu m$ pore size, a porosity of 0.6 is outside the data range, but looks to have a permeability that is $k \approx 2 - 5 \times 10^{-12} m^2$.

An alternative approach is to use the Carman-Kozeny equation

$$k = \frac{1}{72\tau} \frac{\phi^3 D_p^2}{(1-\phi)^2}$$

where $\tau \approx 2$ is tortuosity, the square of the mean path length taken by the air over the total path length, and D_p is the particle diameter, $20 \mu m$. Using $\phi = 0.6$ gives a similar value to the above one, $k = 4 \times 10^{-12} m^2$.

Using $k = 4 \times 10^{-12} m^2$ gives

$$q \approx 0.002 \text{ m s}^{-1}$$

The time for air to move across a $10mm$ array at this speed is about 5 seconds, comparable to

but a little slower than the time taken by the water.

Another time scale of interest is the time taken for water to penetrate down the pillars, which may be estimated by considering the experimental results of Moulinet and Bartolo. Their experiment consisted of depositing a small droplet of water in the Fakir state on a superhydrohpobic surface and monitoring the droplet profile evolution. As evaporation of the droplet ensues the droplet radius decreases. The contact lines recedes and the transition from the Fakir state to Wenzel occurs in less than 20ms. This is relatively fast compared to the speed of the water and the air.

The implication of these timescales is that it is possible for the water to trap air underneath it, as it passes over the array of pillars and then seals off the escape route at the exit. This motivates the more careful examination of the interaction between water and air that appears later in this report.

4 Liquid in contact with a single cylindrical pillar

Consider a single cylindrical pillar and a liquid in contact with the curved surface of the cylinder. In particular we are interested in the shape of the liquid meniscus. The motivation behind considering this problem is that we can get an approximation for how much the water-air will drop in a distance of $10\mu m$ which is half the distance between the centre of the pillars in Stokes' experimental setup. The radius of the cylinder, R is $7.5\mu m$ and the capillary length for water is $2.73 \times 10^{-3} m$. [10] and [11] derived asymptotic solutions to the Young-Laplace for the liquid profile in contact with a single cylindrical pillar. Of particular interest is the inner solution in [11] which is valid in an $O(R)$ boundary layer near the cylinder.

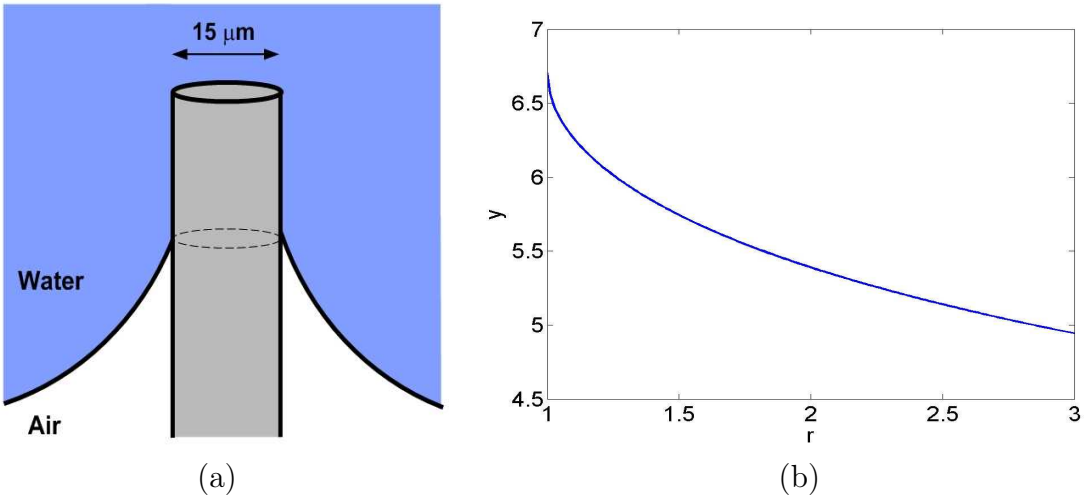

(a) (b)

Figure 7: (a) Schematic of liquid meniscus. (b) Dimensionless plot of liquid height y against distance from cylinder centre, r. We multiply dimensionless quantities by R to convert to dimensional quantities. The contact angle was taken to be $170°$.

For the given parameters, the plot in figure 7 suggests that the water-air interface can drop approximately $12\mu m$ in a distance of $10\mu m$.

5 Partial wetting phenomenon in superhydrophobic microchannels in two dimensions

In this section we study a two-dimensional, Poiseuille flow through a microchannel. Via some geometrical arguments we establish a criterion for which the liquid will go down in between the pillars. Consider the profile of the liquid moving through the channel with velocity u at various instances in time, t_0, t_1, t_2 and t_3.

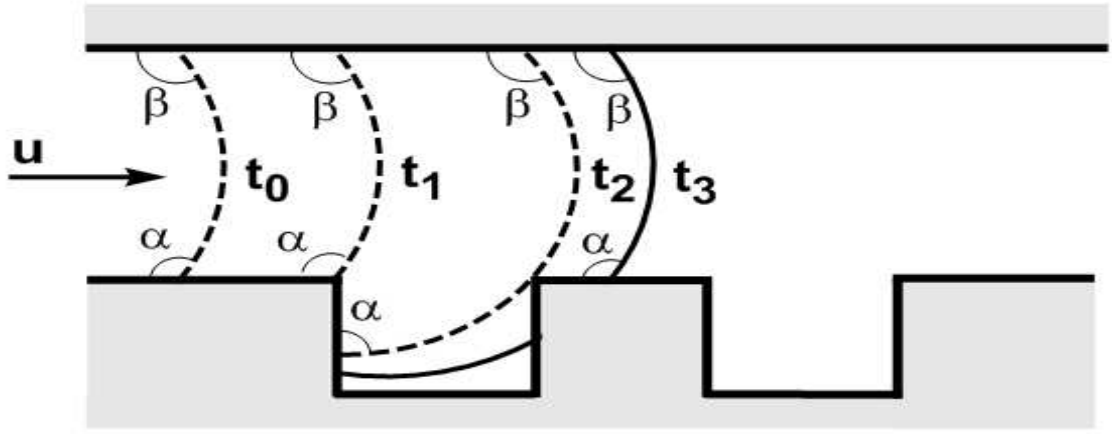

Figure 8: Liquid profile at various times as it flows through the microchannel.

α and β are the liquid-surface contact angles related to the lower and upper channel surfaces, respectively. The equilibrium condition of the free surface is given by

$$\Delta p = \gamma \frac{1}{R}$$

where Δp^* is the pressure difference across the liquid-air interface and R is the radius of curvature. If we consider the circular liquid front in figure (9) and via some geometrical arguments it may be shown that the center of the circle in figure (9) is

$$(x_0, y_0) = (-R\cos\beta, -R\cos\alpha)$$

Hence, the resulting equation of the circle for the liquid front is

$$(x + R\cos\beta)^2 + (y + R\cos\alpha)^2 = R^2 \tag{5.1}$$

Rewriting (5.1) for point $C = (d, D)$, we obtain

$$d = -R\cos\beta + \sqrt{R^2 - (D + R\cos\alpha)^2} \tag{5.2}$$

Points A and B have coordinates $A = (x_A, 0)$ and $B = (0, y_B)$ where

$$x_A = -R\cos\beta + R\sin\alpha, \quad y_B = -R\cos\alpha + R\sin\beta \tag{5.3}$$

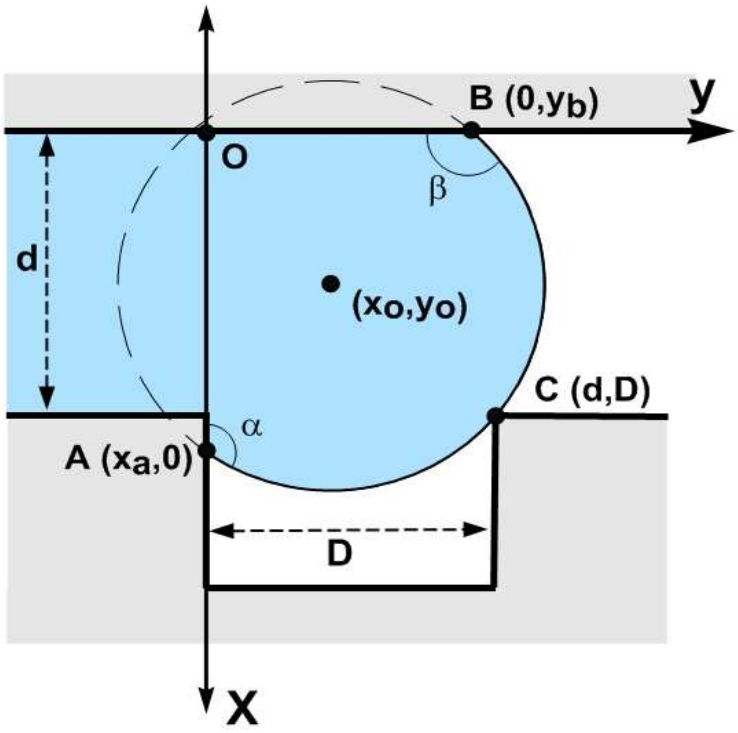

Figure 9: Schematic of liquid going through the microchannel.

The condition necessary for the liquid front to move down the gap between the pillars is $x_A > d$ which may be rewritten using (5.2) and (5.3) to give

$$\frac{d}{D} < \frac{\cos\beta - \sin\alpha}{2\cos\alpha} \tag{5.4}$$

For the case of $\beta = 105^o$ and $\alpha = 105^o$, (5.4) yields

$$d < 2.36D \tag{5.5}$$

Result (5.5) gives us a condition for which the advancing liquid front will go down between the pillars. However, this result only applies to a two-dimensional system and it does not address the influence of the surrounding pillars on the liquid-air interface in three-dimensions.

6 Poiseuille flow across pillars

6.1 Local equilibrium

A mathematical model is now developed for a pressure driven liquid flow through the microchannel across the hydrophobic pillars behind the advancing liquid front. Air can escape between the pillars under the advancing liquid. Assuming that the liquid-air surface is at local equilibrium, we balance the pressure difference across the surface with the surface curvature to get

$$p - \Pi = 2\gamma\kappa \tag{6.1}$$

where p is the liquid pressure, Π is the air pressure, γ is the surface tension and κ is the mean curvature of the liquid-air interface. When the interface is in equilibrium a pressure difference is induced across the interface. We also assume that the liquid-air interface evolves in time as shown in the figure below.

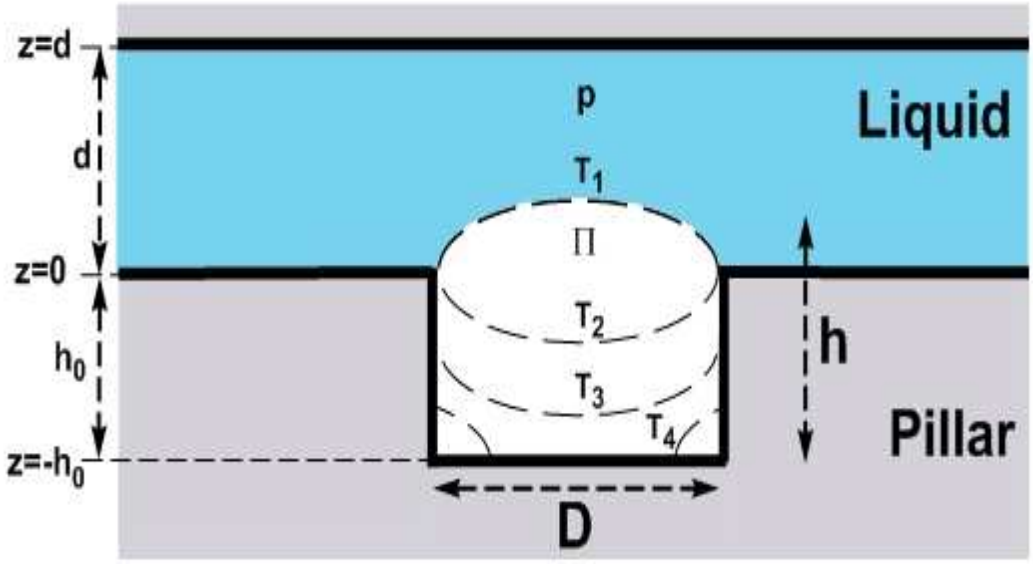

Figure 10: Possible liquid-air interface evolution at times T_1, T_2, T_3 and T_4.

h is the average height of the interface above the base of the pillars and D is the distance between the pillars. At times T_1 and T_2, the liquid-air interface is pinned to top of the pillars at $z = h_0$. At time T_1 the liquid pressure is less than the air pressure. Hence, the liquid-air interface is curved upwards. At some point the liquid pressure becomes greater than the air pressure and the interface becomes curved downwards (as shown at time T_2 in figure (10)).

Increasing liquid pressure causes the interface to move down between the pillars until it reaches the bottom surface between the pillars. At time T_4 the liquid-air interface is pinned to the bottom surface of the microchannel.

6.2 Local equilibrium in relation to theoretical function $f(h)$

Assuming that the liquid-air interface progresses with time as shown in figure (10), we theorize that a suitable equilibrium condition for the interface is

$$p - \Pi = \frac{\gamma}{D} f(h) \tag{6.2}$$

where $f(h)$ is an unknown function of h. With some suitable choice of geometry, interfaces with constant curvature and some physical arguments, the function $f(h)$ can be estimated. Based on figure (10), a plot of $f(h)$ against h will take the form

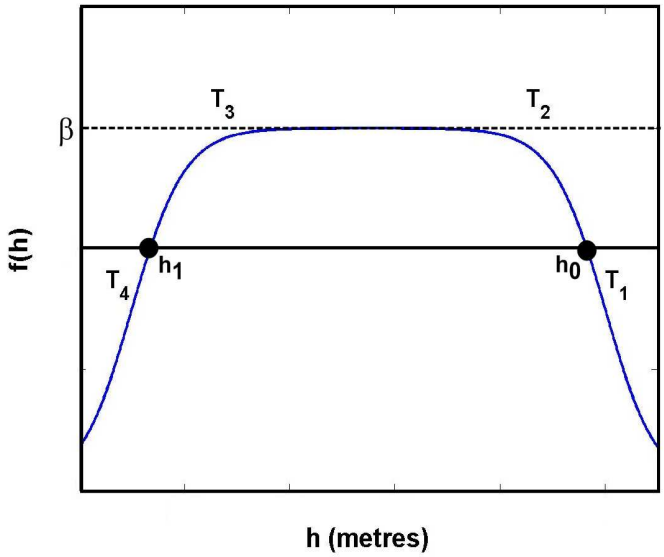

Figure 11: General shape of function $f(h)$.

where $h_0 = (2.5 \times 10^{-5} m)$ is the top of the pillar and h_1 is near the bottom of the pillar. h_1 is the point near the bottom of the pillar where the water-air interface goes from being concave to convex. Figure (11) is just a qualitative description of the function $f(h)$. The main features of the function are briefly discussed here and a more detailed derivation of the function will be

outlined in future work.

At time T_1, $f(h)$ is negative because the pressure difference, $p - \Pi$ is negative. The change of signs of $f(h)$ at h_0 and h_1 are related to the change of signs in the curvature of the liquid-air interface. In the time interval from T_2 to T_3, $f(h)$ and $p - \Pi$ reach their maximum value, β. This occurs while the liquid-air interface is concave and moving down the surface of the pillar. The function in figure (11) was derived via a combination of smooth approximations to the Heaviside function, $H(h)$ of the form

$$H(h) \approx \frac{1}{1 + \exp(-2\,s\,h)} \tag{6.3}$$

where s is a steepness factor used to vary the transition from T_1 to T_2 and T_3 to T_4. Values of h_0, depend on the experimental setup and are easily obtainable. However, exact values of h_1 are not directly available. Further experimental work by the Stokes institute is needed to attain a range of values for h_1.

6.3 Poiseuille flow

We assume that the flow of the fluid through the microchannel takes the form of a Poiseuille flow. d is the height of the channel and l is the length of the channel. A pressure gradient in the x direction is set up in the microchannel due to the pump used in the experiment.

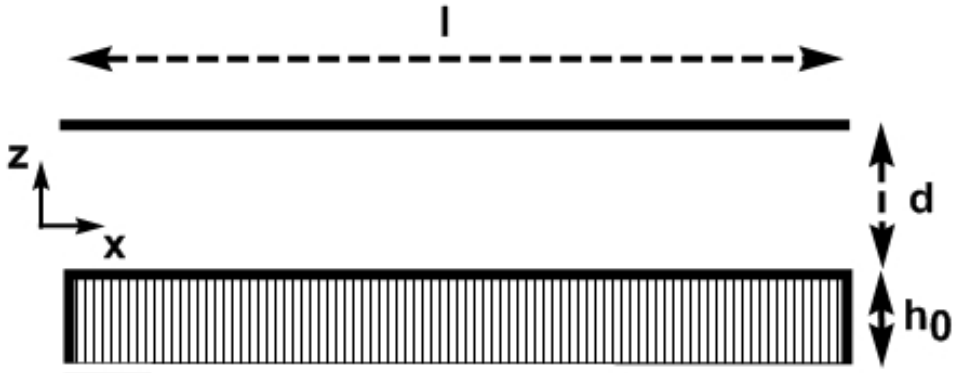

Figure 12: Basic microchannel dimensions.

Deoionised water passes through the microchannel. Water may be classified as a Newtonian, visocous, incompressible fluid. The motion of a Newtonian fluid can be described via the

Navier-Stokes equations. The Navier-Stokes equations are a dynamical statement of the balance of forces acting at any given region of a Newtonian fluid. The complexity of the Navier equations can be reduced significantly via lubrication theory to obtain the thin film equations. Lubrication theory is applicable to the flow of fluids in a geometry in which one length scale is significantly smaller than the other length scale. As the channel height, d is much smaller than the channel length, l, lubrication theory may be used. The resulting governing equation for the velocity in the x direction, u is

$$\frac{\partial p}{\partial x} = \mu_l \frac{\partial^2 u}{\partial z^2} \tag{6.4}$$

where μ_l is the dynamic viscosity of the liquid. Integrating (6.4) twice with respect to z and using the no-slip boundary conditions at $z = 0$ and $z = d$ yields

$$u = \frac{p_x}{2\,\mu_l}\left(z^2 - d\,z \right) \tag{6.5}$$

The vertical velocity component, w is found by substituting (6.5) into the incompressibility condition

$$\frac{\partial u}{\partial x} + \frac{\partial w}{\partial z} = 0$$

and using the no penetration boundary condition at $z = d$, to give

$$w = -\frac{p_{xx}}{2\,\mu_l}\left(\frac{z^3}{3} - \frac{d z^2}{2} + \frac{d^3}{6} \right) \tag{6.6}$$

At the surface of the pillars the downward averaged velocity is

$$w = -\frac{d^3}{12\,\mu_l} p_{xx} \tag{6.7}$$

If we consider the pillars to be a porous medium we can use Darcy's Law to relate the vertical fluid velocity to the pressure difference across the liquid-air interface. Darcy's law describes the flow of a liquid through a porous medium. The law relates the volume flux per unit area (having units of velocity), q to an applied pressure gradient. Hence,

$$q = -\frac{k\,\Pi_x}{\mu_g}\,h \tag{6.8}$$

where k is the effective permeability between the pillars and μ_g is the dynamic viscosity of the air. The downward velocity at the surface of the pillars can be related to the rate at which h is evolving and the pillar-free fraction, ϕ by the equation

$$w = \phi \frac{\partial h}{\partial t} \tag{6.9}$$

If w is negative the fluid is moving downward and the height of the liquid above the pillar base, h is decreasing with time. Whereas, if w is positive the fluid is moving upward and h is increasing with time. The continuity equation for h requires that $\phi\, h_t = -q_x$. Hence, we have

$$w = \phi\, h_t = -\, q_x \tag{6.10}$$

Substituting (6.8) into (6.10) yields

$$-\frac{d^3}{12\,\mu_l} p_{xx} = \phi\, h_t = \frac{k}{\mu_g} \frac{\partial}{\partial x} \Big(h \Pi_x \Big) \tag{6.11}$$

We have the boundary conditions for the liquid pressure and the air pressure

$$\Pi_x = 0\,; \quad p = p_0 + \Delta p\,; \quad \text{at } x = 0 \tag{6.12}$$

$$\Pi = p = p_0\,; \quad \text{at } x = l \tag{6.13}$$

where Δp is the water pressure difference across the length of the channel. Integrating (6.11) once with respect to x leads to

$$-\frac{d^3}{12\,\mu_l} p_x = \frac{k}{\mu_g}\, h \Pi_x + C_1 \tag{6.14}$$

where C_1 is an integration constant. Via the boundary condition for the derivative of the air pressure at $x = 0$, (6.14) reduces to

$$-\frac{d^3}{12\,\mu_l} p_x = C_1$$

Hence, we get

$$C_1 = A\,\frac{d^3}{12\,\mu_l}\frac{\Delta p}{l}$$

where A is an $O(1)$ constant. (6.14) becomes

$$-\frac{d^3}{12\,\mu_l}p_x = \frac{k}{\mu_g}\,h\Pi_x + A\,\frac{d^3}{12\,\mu_l}\,\frac{\Delta p}{l} \tag{6.15}$$

and dividing both sides by $d^3/(12\,\mu_l)$ gives

$$-p_x = M\,h\,\Pi_x + A\frac{\Delta p}{l} \tag{6.16}$$

where $M = (12\,k\,\mu_l)/(d^3\mu_g)$. Rewriting (6.2) in terms of p and differentiating with respect to x leads to

$$p_x = \Pi_x + \frac{\gamma}{D}\,f_x \tag{6.17}$$

Substituting this expression into (6.16) and rearranging in terms of Π_x yields

$$\Pi_x = -\frac{\left(\frac{A\Delta p}{l} + \frac{\gamma}{D}\,f_x\right)}{1 + M\,h} \tag{6.18}$$

Substituting (6.18) into (6.11) gives

$$\phi\,h_t = -\frac{k}{\mu_g}\frac{\partial}{\partial x}\left(\frac{h}{1 + M\,h}\left[\frac{A\Delta p}{l} + \frac{\gamma}{D}\,f'(h)h_x\right]\right) \tag{6.19}$$

which is a nonlinear Richards type equation in h. Richards type equations are typically used to describe water movement in unsaturated soils[12]. Via (6.18) and boundary condition (6.12) we get

$$\frac{A\Delta p}{l} = -\frac{\gamma}{D}\,f'(h)h_x \qquad \text{at } x = 0 \tag{6.20}$$

Now rearranging in (6.17) in terms of Π_x yields

$$\Pi_x = p_x - \frac{\gamma}{D} f_x \tag{6.21}$$

and putting this in (6.16) leads to

$$p_x = -A \frac{\Delta p}{l} \frac{1}{1 + Mh} + \frac{\gamma}{D} \frac{Mh}{1 + Mh} f_x \tag{6.22}$$

Integrating (6.22) over 0 to l gives

$$\int_0^l p_x \, dx = -A \frac{\Delta p}{l} \int_0^l \frac{dx}{1 + Mh} + \frac{\gamma}{D} \int_0^l \frac{Mh}{1 + Mh} f_x \, dx$$

and since $M h \sim 0.1 << 1$, the above expression reduces to

$$\int_0^l p_x \, dx = -A \frac{\Delta p}{l} \int_0^l dx$$

Via the boundary conditions for the liquid pressure, we get $A = 1$. Hence, (6.20) becomes

$$\frac{\Delta p}{l} = -\frac{\gamma}{D} f'(h) h_x \qquad \text{at } x = 0 \tag{6.23}$$

Summary of dimensional problem

The full dimensional problem for the average liquid height may be summarised as follows.

$$\phi \frac{\partial h}{\partial t} = -\frac{k}{\mu_g} \frac{\partial}{\partial x} \left(h \left[\frac{\Delta p}{l} + \frac{\gamma}{D} f'(h) h_x \right] \right) \tag{6.24}$$

$$\frac{\Delta p}{l} = -\frac{\gamma}{D} f'(h) h_x \qquad \text{at } x = 0 \tag{6.25}$$

$$h = h_0 \qquad \text{at } x = l \tag{6.26}$$

Non-dimensionalisation

We define the dimensionless variables

$$h = D\hat{h}; \quad x = l\hat{x}; \quad t = \frac{\phi\, D\, \mu_g\, l^2}{k\gamma}\hat{t}$$

and substituting them into (6.24) leads to

$$\frac{\partial \hat{h}}{\partial \hat{t}} = -\frac{\partial}{\partial \hat{x}}\Big(\hat{h}\Big[\alpha + f'(\hat{h})\,\frac{\partial \hat{h}}{\partial \hat{x}}\Big]\Big) \tag{6.27}$$

where $\alpha = (\Delta p\, D)/\gamma$ is a dimensionless parameter. Boundary conditions (6.25) and (6.26) become

$$-f'(\hat{h})\,\frac{\partial \hat{h}}{\partial \hat{x}} = \alpha \qquad \text{at } \hat{x} = 0 \tag{6.28}$$

$$\hat{h} = \hat{h}_0 \qquad \text{at } \hat{x} = 1 \tag{6.29}$$

where $\hat{h}_0 = h_0/D$.

Steady state solution

Assuming there is a steady state solution for the liquid height, $\hat{h}$, the time derivative term in (6.27) vanishes to give

$$\frac{d}{d\hat{x}}\Big(\hat{h}\Big[\alpha + f'(\hat{h})\,\frac{d\hat{h}}{d\hat{x}}\Big]\Big) = 0 \tag{6.30}$$

Integrating both sides of the above equation with respect to $\hat{x}$ leads to

$$\hat{h}\Big(\alpha + f'(\hat{h})\,\frac{d\hat{h}}{d\hat{x}}\Big) = C_2 \tag{6.31}$$

where C_2 is an integration constant. Via boundary condition (6.28) we get that C_2 equals zero

to give

$$\hat{h}\left(\alpha + f'(\hat{h})\frac{d\hat{h}}{d\hat{x}}\right) = 0 \tag{6.32}$$

which implies that

$$\hat{h} = 0\,; \qquad \text{or} \qquad \alpha + f'(\hat{h})\frac{d\hat{h}}{d\hat{x}} = 0 \tag{6.33}$$

If follows that the solution to (6.33) is

$$f = -\alpha\hat{x} + C_3 \tag{6.34}$$

where C_3 is an integration constant. Using (6.29) we get that

$$f(\hat{h}) = f(\hat{h_0}) = 0 \qquad \text{at } \hat{x} = 1$$

which gives the following two steady state solutions

$$\hat{h} = 0 \tag{6.35}$$
$$f(\hat{x}) = \alpha(1-\hat{x}) \tag{6.36}$$

The first of the steady state solutions simply states that the water-air interface becomes pinned to the top of the pillars and that the interface is horizontal. The second of the steady state solutions is a linear, negative relationship between the function f and the dimensionless length along the microchannel, $\hat{x}$. From (6.2) we have that $f(h) \sim p - \Pi$. Hence, solution (6.36) suggests as $\hat{x}$ decreases, f increases and hence, $p - \Pi$ increases. This increase in the function f is associated with the interval from T_1 to T_2 in figure (10). Thus, solution (6.36) also only explains a steady state scenario where the water-air interface is pinned to the top of the pillar. In addition, while the interface is pinned the curvature of the interface, changes sign. In other words, the interface goes from being concave to convex. Moreover, solution (6.36) does not provide any information about f as a function of h and how the interface evolves as it moves down between the pillars.

To summarise, in the case of $\alpha < \beta$ (were β is the max value of $f(h)$ and the pressure difference across the water-air interface), the steady state solutions only describe cases where the

interface is pinned to the top of the pillar. If Δp, the pressure difference across the length of the microchannel becomes sufficiently large, then $\alpha > \beta$ and the interface will move down in between the pillars. A full time dependent solution of (6.27) is necessary to characterise the interface evolution between the pillars.

7 Conclusions and future work

This report outlines a mathematical model used to describe an experimental setup presented by the Stokes Institute. In particular we are interested in modelling the interaction between a microchannel whose surfaces are superhydrophobic and deionised water flowing through the microchannel subject to a pressure gradient. In section (2) we reviewed the various possible wetting states associated with superhydrophobic surfaces. Section (3) summarises the time scales involved in the process. The key result in this section being that it is possible for air to get trapped amongst the microchannel pillars underneath the advancing water front. In section (4) classical asymptotic results for the shape of liquid meniscus in contact with the curved surface of a cylinder are used to estimate the distance the water-air interface will drop between two pillars. Simple two-dimensional, geometrical arguments in section (5) are used to establish a criteria for which the advancing water front will go down between the pillars. In the final section we considered a pressure driven Poiseuille flow over the top of the pillars. Lubrication theory provided the downward velocity of the water at the top of the pillars. This result along with Darcy's Law was used to derive a nonlinear Richards type equation for the average water-air interface height. Steady state solutions were derived and the validity of these solutions was discussed.

Future work will include a more thorough derivation of the function $f(h)$ which is proportional to the pressure difference across the water-air interface, $p - \Pi$. $f(h)$ may be approximated via hyperbolic functions of the form (6.3). More careful analysis and collaboration with the Stokes Institute is required to determine the exact nature of the function $f(h)$. A full time dependent solution to equation (6.27) is also desirable as the steady state solutions do not provide a sufficient description of the water-air interface progression between the pillars. Finally, this report does not account for the effect of the scallops on the surface of the pillars in determining the water-air contact line. Any future model must address the interaction between the scallops and the water-air interface.

Acknowledgments

We acknowledge the support of the Mathematics Applications Consortium for Science and Industry (www.macsi.ul.ie) funded by the Science Foundation Ireland mathematics initiative grant 06/MI/005.

Nomenclature

(x, y, z)	Cartesian coordinates vector		m
$\mathbf{u} = (u, v, w)$	Velocity vector		ms^{-1}
(p, Π)	(Water/air) pressure		Nm^{-2}
κ	Curvature		m^{-1}
h	Average height of liquid above pillars		m
ϕ	Pillar free fraction		ND
t	Time		s
q	Height flux		ms^{-1}
(b, l, d)	Microchannel (breadth/length/height)	$(10^{-2}/10^{-2}/8 \times 10^{-5})$	m
(R, h_0)	Pillar (radius/height)	$(7.5 \times 10^{-6}/2.5 \times 10^{-5})$	m
D	Gap between pillars (centre to centre)	2×10^{-5}	m
U	Water velocity	0.012	ms^{-1}
L_c	Capillary length of water	2.73×10^{-3}	m
γ	Surface tension of water	0.073	Nm^{-1}
θ	Contact angle		ND
(μ_l, μ_g)	(Water/air) dynamic viscosity	$(8.9 \times 10^{-4}/1.8 \times 10^{-5})$	$kg\,m^{-1}s^{-1}$
k	Permeability	4×10^{-12}	m^2
Δp	Water pressure difference across	100	Pa
	the array	100	Pa
α	$(\Delta p\, D)/\gamma$	0.0274	ND
β	Maximum $f(h)$ value		
$\hat{h}_0$	h_0/D	1.25	ND

Bibliography

[1] J .Zhang and D.Y. Kwok. Contact line and contact angle dynamics in superhydrophobic channels *Langmuir*, 22(11):4998-5004, 2006.

[2] A. Dupuis and Y.M. Yeomans, Modeling droplets on superhydrophobic surfaces: equilibrium states and transitions. *Langmuir*, 21(6):2624-2629, 2005.

[3] C. Dorrer and Rühe. Some thoughts on superhydrophobic wetting. *Soft Matter*, 5(1):51-61, 2008.

[4] R. Enright, T. Dalton, T.N. Krupenkin et al. Effects of interfacial position on drag reduction in a superhydrophobic microchannel. *6th Int. Conf. Nanochannels, Microchannels, and Minichannels*, June 23-25:835-845, 2008.

[5] T. Young, An essay on the cohesion of fluids, *Philos. T. Roy. Soc. Lon.*, 95:65-87, 1805.

[6] S. Wang and L. Jiang, Definition of superhydrophobic states. *Adv. Mater.*, 19:3423-3424, 2007.

[7] R.N.Wenzel. Resistance of solid surfaces to wetting by water. *Ind. Chem. Eng.*, 28(8):988-995, 1936.

[8] A.B.D. Cassie and S. Baxter. Wettability of porous surfaces. *Trans. Faraday Soc.*, 40:546-551, 1944.

[9] S. Moulinet and D. Bartolo, Life and death of a fakir droplet: Impalement transitions on superhydrophobic surfaces. *Eur. Phys. J. E*, 24(3):251-260, 2007.

[10] D. James. The meniscus on the outside of a small circular cylinder. *J. Fluid Mech.*, 63(4):657-664, 1974.

[11] L.L. Lo. The meniscus on a needle - a lesson in matching. *J. Fluid Mech.*, 132:65-78, 1983.

[12] L.A. Richards. Capillary conduction of liquids through porous mediums. *Physics 1*, 318:318-333, 1931.